Journal of Power Sources 185 (2008) 1550–1556

Contents lists available at ScienceDirect

Journal of Power Sources

journal homepage: www.elsevier.com/locate/jpowsour

Annealed Mn–Fe binary oxides for supercapacitor applications

Ming-Tsung Lee, Jeng-Kuei Chang*, Yao-Tsung Hsieh, Wen-Ta Tsai

Department of Materials Science and Engineering, National Cheng Kung University, 1 University Road, Tainan City 701, Taiwan

ARTICLE INFO

Article history:
Received 10 July 2008
Received in revised form 4 September 2008
Accepted 4 September 2008
Available online 12 September 2008

Keywords:
Mn–Fe binary oxide
Annealing
Heat treatment
Supercapacitor

ABSTRACT

Mn–Fe binary oxide, which is a promising electrode material for use in supercapacitors, is prepared by anodic deposition in mixed manganese acetate and iron chloride plating solution. Tailoring the material characteristics and thus the electrochemical performance of the oxide is attempted by annealing (up to 700 °C in air). The thermal properties of the as-deposited oxide are examined by thermogravimetric and differential thermal analyses. Glancing angle X-ray diffraction (GAXRD), scanning electron microscopy, and X-ray photoelectron spectroscopy (XPS) are used to examine the crystal structure, surface morphology, and chemical state, respectively. Dehydration, organic-matter decomposition, oxidation, surface morphology reconstruction, and crystallization of the oxide as a function of annealing temperature are investigated. The 100 °C-annealed oxide, evaluated by cyclic voltammetry at a potential sweep rate of 5 mV s^{-1}, shows an optimum specific capacitance of 280 F g^{-1}. Cyclic stability of the oxide electrode can also be improved by post-heat treatment. However, the binary oxide loses its pseudocapacitive capability at the annealing temperature of 500 °C, at which point the formation of crystalline $(Mn–Fe)_2O_3$ occurs.

1. Introduction

Supercapacitors are charge storage devices that have a greater power density and longer cycle life than batteries have, and a higher energy density than that of conventional capacitors [1]. Accordingly, they have been developed for a range of applications, such as in hybrid electric vehicles, consumer electronics, medical electronics, and military missile systems. Supercapacitors can be classified, based on their operating mechanisms, into two categories: (1) double-layer capacitors, which are based on non-faradic charge separation at the electrode/electrolyte interface; and (2) pseudocapacitors, which are based on the faradic redox reaction of electroactive materials. Hydrous ruthenium oxide has been demonstrated to exhibit ideal pseudocapacitive behavior and is a great electrode material for use in supercapacitors [2]. A strong dependence of its specific capacitance on the crystal structure, governed by annealing temperature, was reported [3]. The largest specific capacitance (over 700 F g^{-1}), with excellent reversibility, of the oxide was obtained at 150 °C, which is just below the crystallization temperature. However, the high cost of ruthenium has limited its commercial use. Finding a cheaper alternative with equivalent pseudocapacitive characteristics is thus attracting a lot of attention.

Manganese (Mn) oxide is considered one of the most promising electrode materials for supercapacitor applications due to its satisfactory electrochemical performance and its natural abundance and environmental compatibility. Its preparation methods include electrodeposition [4–7], thermal decomposition [8], co-precipitation [9–12], sol–gel processes [13–16], physical vapor deposition [17,18], and hydrothermal synthesis [19,20]. Recently, several researchers have begun to study the effects of post-heat treatment on prepared Mn oxide [13–15,21–24]. It was found that material properties and pseudocapacitive performance of Mn oxide as a function of annealing temperature varied with the preparation process adopted. For example, Lin et al. [24] synthesized Mn oxide using a sol–gel method. The prepared sample remained amorphous until 200 °C but crystallized at 250 °C. In the annealing temperature range of 250–500 °C, both crystalline Mn_3O_4 and Mn_2O_3 phases were noticed. The highest specific capacitance was found at 300 °C, probably due to high porosity. However, our previous study [21] indicated that, for anodically deposited Mn oxide, the crystallization reaction (to form Mn_2O_3) occurred at 500 °C. At a low annealing temperature (≤200 °C), the specific capacitance decreased and cyclic stability increased with increasing heating temperature. A significant degradation in pseudocapacitive performance was recognized at 300 °C, a temperature at which morphological reconstruction took place.

In order to further improve the pseudocapacitive performance of plain Mn oxide, addition of other transition metal oxides has been attempted. Studies have reported that Ni [11,25], Pb [11], Co [25–28], Mo [29], and V [30] oxides addition could have beneficial effects. We also proposed [31] that Mn–Fe oxide, in which Mn oxide was nanocrystalline and Fe oxide was amorphous, could be

* Corresponding author. Tel.: +886 6 2757575x62942; fax: +886 6 2754395.
E-mail address: catalyst@mail.mse.ncku.edu.tw (J.-K. Chang).

0378-7753/$ – see front matter © 2008 Elsevier B.V. All rights reserved.
doi:10.1016/j.jpowsour.2008.09.007

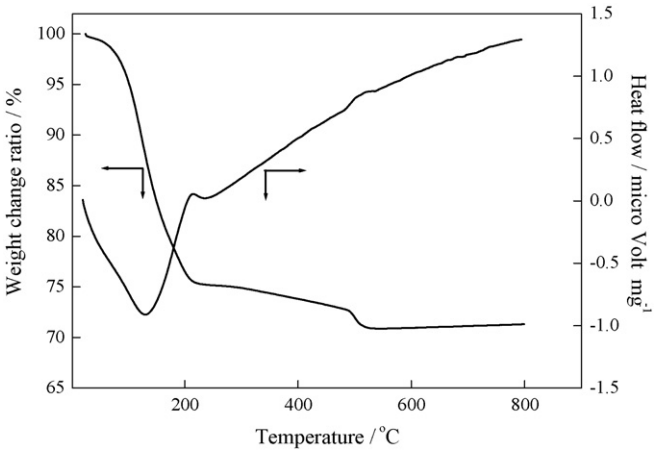

Fig. 1. TG/DT plot of anodically deposited Mn–Fe binary oxide measured at a heating rate of 10 °C min^{-1} in an air atmosphere.

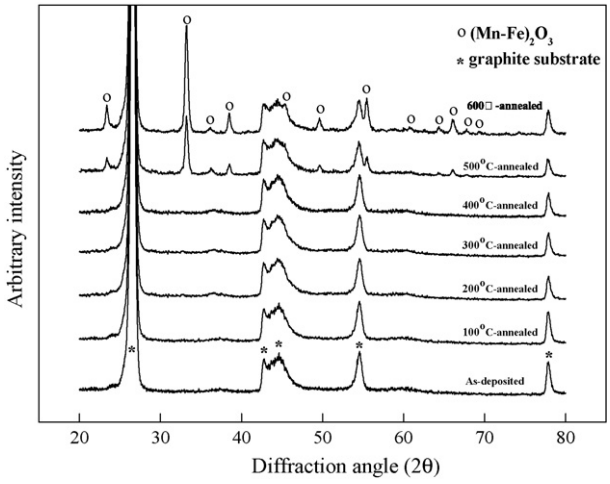

Fig. 2. X-ray diffraction patterns of the Mn–Fe binary oxide electrodes annealed at various temperatures.

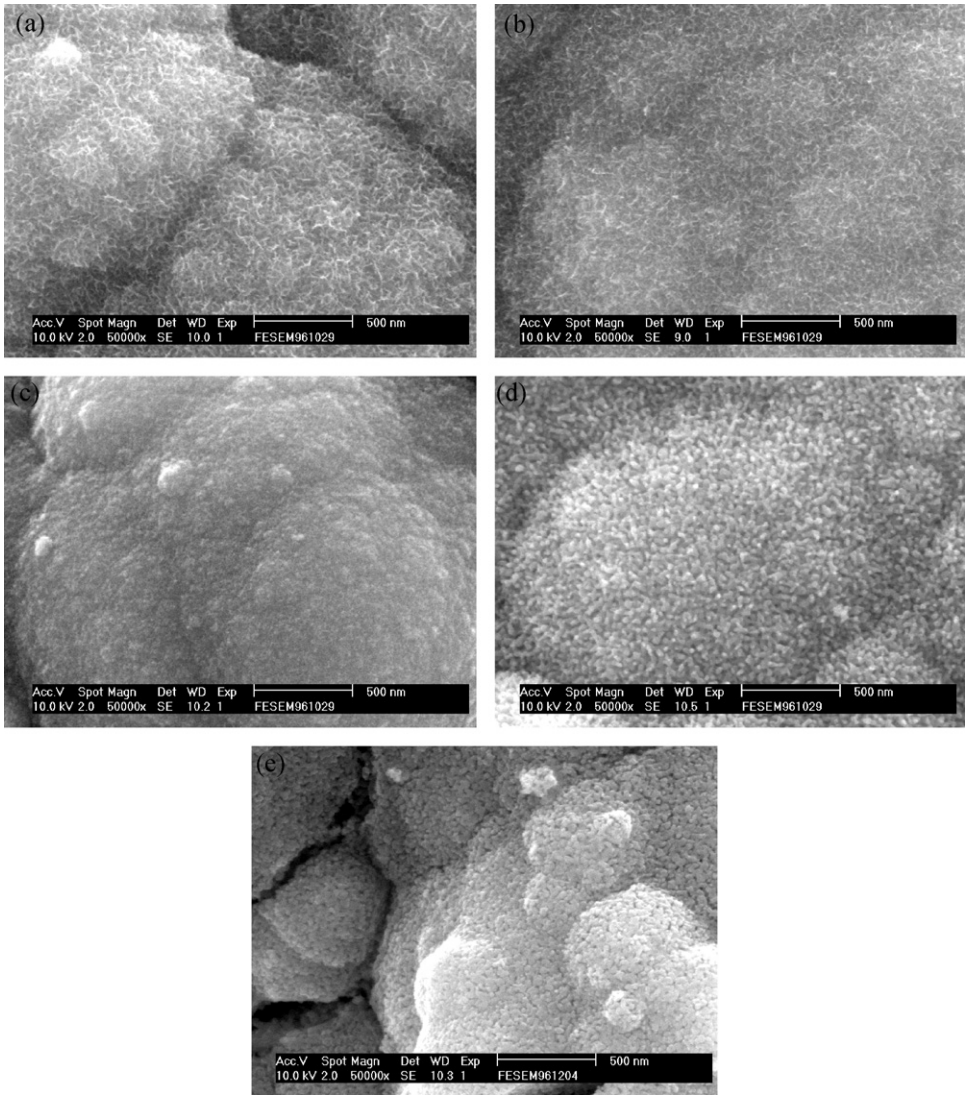

Fig. 3. SEM micrographs of the (a) as-deposited, (b) 100 °C-annealed, (c) 300 °C-annealed, (d) 500 °C-annealed, and (e) 700 °C-annealed Mn–Fe binary oxide electrodes.

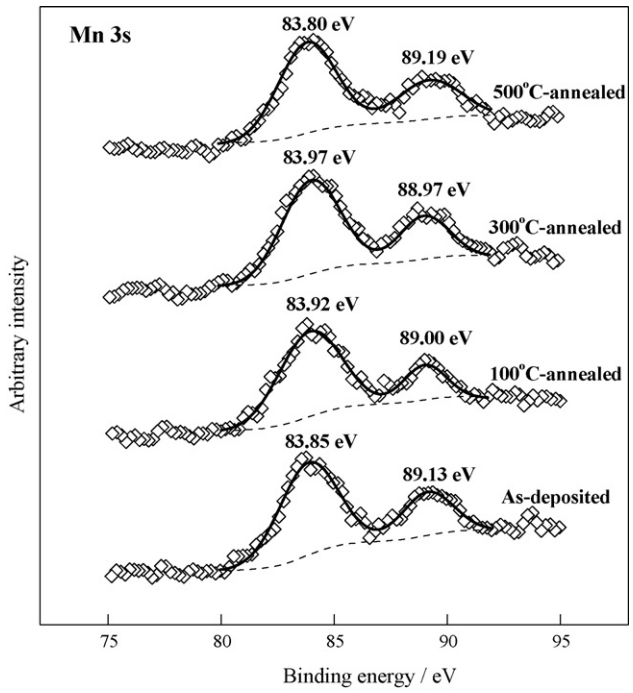

Fig. 4. XPS spectra of Mn 3s orbit for the Mn–Fe binary oxide annealed at various temperatures.

prepared by anodic deposition. With proper Fe addition, specific capacitance of the binary oxide was enhanced by 21%; the cyclic stability can also be significantly improved. However, the effects of heat treatment, though very important, have not been explored yet. In the present study, material characteristics and the corresponding electrochemical behavior of Mn–Fe binary oxide as a function of annealing temperature were systematically investigated. Optimizing the post-heat temperature to tailor supercapacitor performance of the binary oxide electrode was attempted as well.

2. Experimental methods

Binary Mn–Fe oxide was electroplated onto 1 cm × 1 cm graphite substrates, which have a resistivity of 12 μΩ m and an average grain size of 10 μm, by anodic deposition in a mixed plating solution of 0.25 M $Mn(CH_3COO)_2$ and 0.05 M $FeCl_3$ at 25 °C. The substrates were first polished with SiC paper of 800 grit, then degreased with acetone and water, etched in 0.2 M H_2SO_4, and finally washed with pure water in an ultrasonic bath. During the deposition, the graphite substrate was held as the anode, and a platinum sheet was used as the counter electrode. In addition, a saturated calomel electrode (SCE) was assembled as the reference electrode. Anodic deposition was performed using an EG&G Princeton Applied Research model 263 potentiostat at a constant applied potential of 0.8 V (versus SCE) to give a total passed charge of 1.5 C. The Fe to Mn atomic ratio in the deposited oxide was approximately 1:9 [31]. The weight change of the electrode before and after deposition was measured using a microbalance with an accuracy of 1×10^{-4} g; a typical mass of the loading oxide was found to be about 1.1 mg. A Netzsch STA 409 analyzer was used to perform simultaneous thermogravimetric and differential thermal (TG/DT) analyses of the deposited binary oxide, which was detached from the graphite substrate. The sample was heated from 25 °C to 800 °C at a rate of 10 °C min^{-1} under a flowing air atmosphere. The air flow rate was 20 mL min^{-1}.

The binary oxide electrodes were annealed at various temperatures (up to 700 °C in air) for 2 h in a tube furnace. The crystal structure of the oxide was determined by glancing angle X-ray diffraction (GAXRD). The patterns were recorded on a Rigaku D/MAX-2500 diffractometer with a glancing incident angle of 1°. Cu Kα radiation with a wavelength of 1.5418 Å was used as the X-ray source. The detected diffraction angle (2θ) was scanned from 20° to 80° with a speed of 4° min^{-1}. The surface morphologies of the electrodes were observed by means of a scanning electron microscope (SEM, Philip XL-40FEG). X-ray photoelectron spectroscopy (XPS) was used to examine the chemical state of the oxides. The measurements were performed with a spectrometer (JOEL JPS 9010 MX) with Mg Kα radiation (1253.6 eV) as the X-ray source. The pressure in the main chamber was approximately 1×10^{-9} Torr during the analyses.

The electrochemical behavior of the as-deposited and the annealed oxides was characterized by cyclic voltammetry (CV) in 2 M KC1 solution at room temperature. A three-electrode cell, in which the oxide electrode was assembled as the working electrode, was adopted. A flat platinum sheet with a surface area of 10 cm^2 and an SCE were used as the counter electrode and the reference electrode, respectively. The electrode potential was scanned at various rates (from 5 mV s^{-1} to 100 mV s^{-1}) within a potential range of 0–1 V. Electrochemical stability of the oxide electrode was evaluated by repeating the CV scan for 500 cycles. The variation of the oxide capacitance versus the cycle number was recorded.

3. Results and discussion

3.1. TG/DT analyses

Fig. 1 shows a TG/DT plot of the deposited binary oxide, which was detached from the substrate, measured in an air atmosphere. The weight and enthalpic changes as a function of temperature are demonstrated in this figure. The initially sharp weight loss, corresponding to an endothermic reaction, was found around 100 °C. This can be attributed to the release of adsorbed water. As the temperature was increased to 200 °C, the weight loss rate slightly decreased and an associated exothermic peak was observed. This

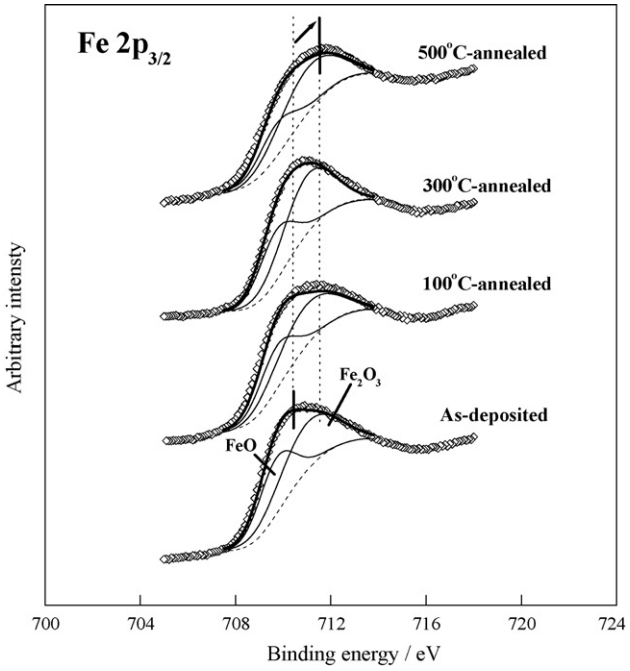

Fig. 5. XPS spectra of Fe $2p_{3/2}$ orbit for the Mn–Fe binary oxide annealed at various temperatures.

Table 1
XPS analytical results of the anodically deposited Mn–Fe binary oxide as a function of annealing temperature

Sample	Mn 3s			Fe $2p_{3/2}$		O 1s	
	E_1 (eV)	E_2 (eV)	ΔE	Species	Peak area (%)	Species	Peak area (%)
As-deposited	83.85	89.13	5.28	FeO	43%	M–O–M	44%
						M–O–H	41%
				Fe_2O_3	57%	H–O–H	15%
100 °C-annealed	83.92	89.00	5.08	FeO	39%	M–O–M	55%
						M–O–H	36%
				Fe_2O_3	61%	H–O–H	9%
300 °C-annealed	83.97	88.97	5.00	FeO	35%	M–O–M	71%
						M–O–H	21%
				Fe_2O_3	65%	H–O–H	8%
500 °C-annealed	83.80	89.19	5.39	FeO	27%	M–O–M	76%
						M–O–H	17%
				Fe_2O_3	73%	H–O–H	7%
Standard species [34]							
MnO							5.79
Mn_3O_4							5.50
Mn_2O_3							5.41
MnO_2							4.78

was ascribed to the decomposition of some organic species from the acetate-based plating solution. The approximately constant weight in the intermediate temperature range of 200–500 °C was due to a balance between a loss of structural water and a further oxidation of the oxide, as reported in the literature [32]. A stepped weight loss along with an exothermic peak, attributed to oxygen release from Mn oxide [11,32,33], is clearly discernible at 500 °C. Beyond this temperature, the oxide weight plateaued until 800 °C.

3.2. Crystal structure

The GAXRD patterns of the binary oxide electrodes annealed at various temperatures are shown in Fig. 2. The patterns of the samples annealed up to 400 °C are identical to that of the as-deposited oxide electrode. All the strong diffraction peaks are associated with the graphite substrate. It should be noted that the oxide only contributed a broadened peak with very low intensity near 37° in each pattern, revealing poor crystallinity until 400 °C. When the annealing temperature increased to 500 °C, formation of a highly crystalline $(Mn–Fe)_2O_3$ solid solution phase (JCPDS 08-0010) was recognized. The crystallization reaction that occurred at 500 °C coincided with the stepped weight loss observed in Fig. 1. When the temperature was further elevated to 700 °C, the GAXRD pattern did not significantly change, except that the diffraction intensity from $(Mn–Fe)_2O_3$ became stronger than obtained at 500 °C, indicating that the crystalline phase was further developed. Our previous study [21] indicated that plain Mn oxide prepared by anodic deposition crystallized at 500 °C to form Mn_2O_3, which was further transformed to Mn_3O_4 at 700 °C. The analytical results in this work suggest that the incorporation of Fe seems to stabilize $(Mn–Fe)_2O_3$, and thus hinders the phase transformation at 700 °C.

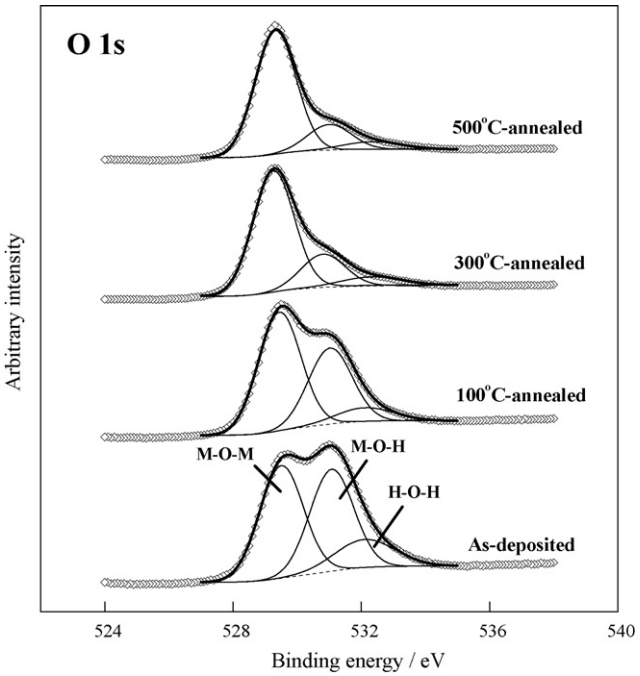

Fig. 6. XPS spectra of O 1s orbit for the Mn–Fe binary oxide annealed at various temperatures.

3.3. Surface morphology

Fig. 3 shows the surface morphologies of the oxide electrodes examined by SEM. As revealed in Fig. 3(a), the as-deposited sample consists of numerous nanoscale fibers in a three-dimensional network. For the 100 °C-annealed electrode (exhibited in Fig. 3(b)), since the adsorbed water was removed, the fibrous oxide gradually becomes shorter and tends to join together. Fig. 3(c) demonstrates the oxide annealed at 300 °C. Due to the release of organic species and further oxidation of the oxide (as mentioned previously), a fused and condensed morphology is observed. Fig. 3(d) shows a micrograph of the 500 °C-annealed oxide, revealing that it is composed of spherical nano-size particles. The apparent change in morphology was associated with the crystallization reaction of the deposited binary oxide, since the formation of the crystalline $(Mn–Fe)_2O_3$ phase was confirmed by GAXRD. When the annealing temperature was increased to 700 °C, as illustrated in Fig. 3(e), the growth of the crystal size was recognized. The cracks observed are probably caused by shrinkage stress during drying.

3.4. Chemical state

The chemical state variation of the binary oxide as a function of annealing temperature was examined using XPS. Fig. 4 shows the

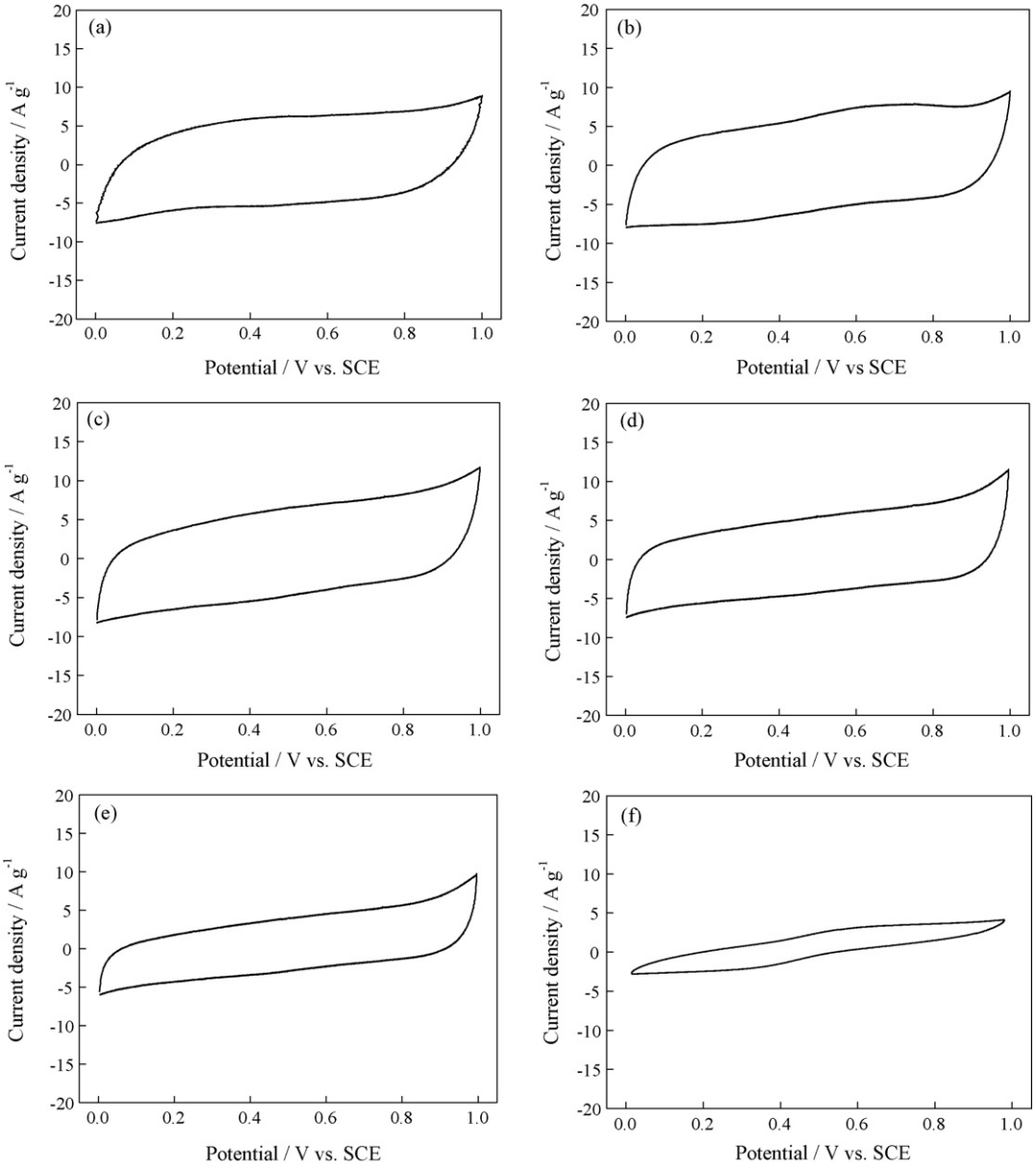

Fig. 7. Cyclic voltammograms of (a) as-prepared, (b) 100 °C-annealed, (c) 200 °C-annealed, (d) 300 °C-annealed, (e) 400 °C-annealed and (f) 500 °C-annealed Mn–Fe binary oxide electrodes, measured in 2 M KC1 solution with a potential scan rate of 25 mV s^{-1}.

spectra for the Mn 3s orbit of the various electrodes. It is known that the Mn valence can be identified by measuring the multiplet splitting width of the Mn 3s XPS peaks [34,35]. The exchange interaction between the core level electron (3s) and the unpaired electrons in the valence band level (3d) results in the peak separation of the Mn 3s spectrum upon photoelectron ejection [36,37]. Accordingly, the lower valence of Mn gives rise to a wider splitting of the 3s peaks. As shown in Fig. 4, the splitting width of Mn 3s peaks varies with annealing temperature. The peak locations and separation width (ΔE) derived from Gauss fitting results are listed in Table 1. Multiplet splittings of Mn 3s for pure MnO, Mn_3O_4, Mn_2O_3 and MnO_2, which were reported by Chigane and Ishikawa [34], are also shown in this table for comparison. The peak separation of the as-deposited binary oxide is 5.28 eV, indicating that trivalent and tetravalent Mn coexist within the oxide. A gradual decrease in ΔE was found when the annealing temperature was increased (5.08 eV at 100 °C and 5.00 eV at 300 °C). This confirms that further oxidation of Mn oxide (approaching +4 valence) occurred in this temperature range. When the oxide was annealed at 500 °C, a sudden increase in the peak separation width was observed. The ΔE of 5.39 eV suggests the formation of Mn_2O_3 (accompanied by oxygen release), which is consistent with previous GAXRD and TG/DT analyses.

Fig. 5 shows the Fe $2p_{3/2}$ XPS spectra of the various oxides. A peak shift toward a higher binding energy with increasing annealing temperature is clearly found, implying a change in the Fe chemical state. To describe the variation more specifically, Gauss curve fitting of the obtained XPS curves was performed. As demonstrated in this figure, each spectrum is composed of two components associating the signals from FeO (at 709.7 eV) and Fe_2O_3 (at 711.0 eV) [38,39]. The peak areas (measured as a percentage of the total area under the respective Fe $2p_{3/2}$ spectrum) that correlate with the relative amounts of FeO and Fe_2O_3 in the oxides are summarized in Table 1. A monotonous increase in the Fe oxidation state (from bivalence to trivalence) with increasing annealing temperature is clearly visible.

The O 1s spectra of the as-deposited binary oxide and the oxides annealed at various temperatures were also analyzed; the results are shown in Fig. 6. As demonstrated, the spectra obtained can be deconvoluted into three constituent peaks that correspond to different oxygen-containing species [34,35], which are metal oxide (M–O–M, M includes Mn and Fe) at around 529.8 eV, metal hydroxide (M–O–H) at around 531.0 eV, and water (H–O–H) at around 532.3 eV. It was difficult to distinguish between the Mn bond and the Fe bond because the difference in the binding energy between these two bonds is less than the resolution limit. The peak area ratios of the three species for the various oxides are summarized in Table 1. After annealing at 100 °C, the amounts of hydrous oxide (i.e., M–O–H) and water significantly decreased, indicating that dehydration of the deposited oxide occurred. When the heating temperature was increased from 100 °C to 300 °C, a further reduction of the hydrous oxide was clearly recognized while the water content slightly decreased. At the temperature of 500 °C, at which the crystallization reaction took place (according to GAXRD analyses), the anhydrous form (Mn–O–Mn) was the dominant species in the oxide.

3.5. Electrochemical characteristics

The electrochemical performance of the oxide electrodes was evaluated by CV. Fig. 7 shows the obtained voltammograms, measured in 2 M KCl aqueous electrolyte, with a potential scan rate of 5 mV s^{-1}. At annealing temperatures of up to 400 °C, as shown in Fig. 7(a)–(e), the CV curves of the electrodes are symmetric in anodic and cathodic areas. The CV response current remained nearly constant during forward and backward scans but immediately changed its flow direction when the potential was switched to be in reverse. The results reveal the excellent reversibility and ideal pseudocapacitive behavior of the electrodes. However, the CV curve of the oxide electrode annealed at 500 °C (see Fig. 7(f)) exhibits a quite different electrochemical property. The current was not only in a lower intensity compared to the other electrodes, but also varied with the potential. At this annealing temperature, the formation of the crystalline $(Mn–Fe)_2O_3$ phase was confirmed by GAXRD analysis (Fig. 2). Since the crystal lattice is rigid and not easily expanded (or contracted), retardation of the protonation (or de-protonation) reaction of the oxide can be expected. Therefore, the fast, continuous, and reversible faradaic reaction of the electrode was hindered, causing the loss of pseudocapacitive characteristics.

Fig. 8 presents the CV curves, measured at a potential scan rate of 100 mV s^{-1}, of the as-deposited and the annealed (up to 300 °C) oxide electrodes. As shown, even at such a high potential scan rate, the rectangular shapes and mirror-image characteristics of the four electrodes can still be achieved. The satisfactory kinetic reactivity makes the binary oxides promising electrode materials for high-power supercapacitor applications. However, as can be seen in Fig. 8, the enclosed areas of the CV curves are different, indicating the superior charge storage capability of the oxide annealed at 100 °C. The specific capacitance (C) of the oxide electrode can be quantitatively calculated according to the following equation:

$$C = \frac{\text{specific voltammetric charge}}{\text{potential range}} \quad (1)$$

The specific voltammetric charge (based on the mass of the oxide) was integrated from both the anodic and cathodic CV sweeps. Table 2 lists the specific capacitances, calculated from the average of the anodic and cathodic charge, of the various oxide electrodes measured at different CV scan rates. Since the pseudocapacitive performance results from the electrochemical redox reaction of the oxide, the monotonous decline in capacitance with increasing potential scan rate, due to the kinetic limitation, was clearly observed. The internal potential drop (or iR drop) of the electrode and diffusion limitation of reactants and productants near the electrode/electrolyte interface also caused the capacitance decay at high potential scan rates. The specific capacitances, at a scan rate of 5 mV s^{-1}, of the as-deposited, 100 °C-, 200 °C-, and 300 °C-annealed oxides were 255 F g^{-1}, 280 F g^{-1}, 242 F g^{-1}, and 225 F g^{-1}, respectively. As clearly shown in Table 2, the oxide annealed at 100 °C had the highest specific capacitance among the electrodes at every CV scan rate. The superior performance of the 100 °C-annealed oxide can be attributed to two major factors. (1) Low water content: as confirmed by TG/DT and XPS analyses, absorbed water of the deposited oxide is mainly released under 100 °C. The removal of the electro-inactive species, which cannot contribute to pseudocapacitance, from the oxide leads to an overall improvement of the specific charge storage performance. (2) Optimum hydrous state: it has been reported [11,40,41] that increasing the hydrous state can promote the ionic conductivity but decreases the electronic conductivity of the oxide. The appropriate amount of the hydroxide at 100 °C (in Fig. 6) could be optimum for approaching a better pseudocapacitive property.

Table 2
Specific capacitance (F g^{-1}) of the as-deposited and annealed Mn–Fe binary oxide electrodes at different CV scan rates

Sample	CV scan rate				
	5 mV s^{-1}	10 mV s^{-1}	25 mV s^{-1}	50 mV s^{-1}	100 mV s^{-1}
As-deposited	255	230	212	192	158
100 °C-annealed	280	257	233	215	176
200 °C-annealed	242	220	202	180	150
300 °C-annealed	225	207	193	171	142

Annealing temperatures higher than 100 °C give rise to a significant reduction in the hydrous state, and thus remarkably decrease the ionic conductivity. In the meanwhile, the condensation of the oxide (in Fig. 3(c)) lowers the reactivity and hinders the accessibility of the electrolyte. Moreover, annealing leads to further oxidation of the oxide. It was reported [5] that a higher oxidation state was detrimental to oxide specific capacitance, probably because only a smaller oxidation state change could be achieved during the charge–discharge process [42,43]. The above-mentioned facts explain the capacitance decay for the oxides annealed at 200 °C and 300 °C.

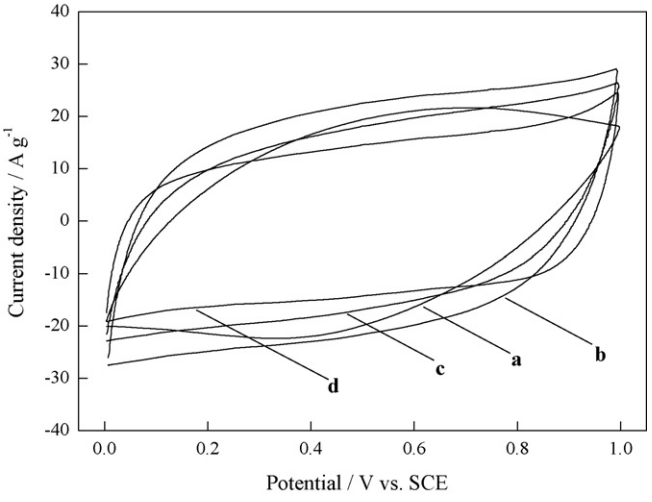

Fig. 8. Cyclic voltammograms of as-prepared (curve a), 100 °C-annealed (curve b), 200 °C-annealed (curve c), and 300 °C-annealed (curve d) Mn–Fe binary oxide electrodes, measured in 2 M KC1 solution with a potential scan rate of 100 mV s^{-1}.

The electrochemical stability of the binary oxide electrodes was evaluated by repeating the CV scan at a potential scan rate of 25 mV s^{-1}. The capacitance retained ratios after 500 cycles (capacitance at the 500th cycle/capacitance at the 1st cycle) of the as-deposited, 100 °C-, 200 °C-, and 300 °C-annealed electrodes were 86%, 95%, 96%, and 97%, respectively. While we previously reported that the addition of Fe oxide effectively increased the capacitance retained ratio of Mn oxide after cycling [31], the present study confirms that the electrochemical stability of the binary oxide can be further improved with post-heat treatment. The 100 °C-annealed Mn–Fe oxide is apparently a promising electrode material for use in high-capacity and long-life supercapacitors.

4. Conclusions

Anodically deposited Mn–Fe binary oxide is poorly crystalline and has a fibrous structure. After annealing at 100 °C, the adsorbed water, which is not electroactive, is removed. At this temperature, the hydrous state of the oxide is also optimized, compromising the ionic and electronic conductivity, and thus producing the best pseudocapacitive performance. When the annealing temperature is increased to 300 °C, the oxidation states of Mn and Fe in the relatively anhydrous oxide increase, while the fibrous oxide tends to condense into blocks; both lead to the degradation of the oxide specific capacitance. At 500 °C, some of the oxygen within the oxide is released, causing weight loss, and a crystallization reaction occurs. The formation of the crystalline $(Mn–Fe)_2O_3$ results in a loss of pseudocapacitive capability. This study shows that the Mn–Fe binary oxide electrode, which undergoes proper post-heat treatment (∼100 °C), has a high-capacity and a long-life, making it ideal for supercapacitor applications.

Acknowledgements

The authors would like to thank the National Science Council of the Republic of China for financially supporting this research (under contract no. NSC 95-2221-E-006-192).

References

[1] B.E. Conway, Electrochemical Supercapacitors, Kluwer-Plenum, New York, 1999.
[2] J.P. Zheng, T.R. Jow, J. Electrochem. Soc. 142 (1995) L6–L8.
[3] J.P. Zheng, P.J. Cygan, T.R. Jow, J. Electrochem. Soc. 142 (1995) 2699–2703.
[4] C.C. Hu, T.W. Tsou, Electrochem. Commun. 4 (2002) 105–109.
[5] J.K. Chang, W.T. Tsai, J. Electrochem. Soc. 150 (2003) A1333–A1388.
[6] N. Nagarajan, H. Humadi, I. Zhitomirsky, Electrochim. Acta 51 (2006) 3039–3045.
[7] J.K. Chang, C.H. Huang, W.T. Tsai, M.J. Deng, I.W. Sun, J. Power Sources 179 (2008) 435–440.
[8] H.Y. Lee, V. Manivannan, J.B. Goodenough, Comptes Rendus Chimie 2 (1999) 565–577.
[9] H.Y. Lee, J.B. Goodenough, J. Solid State Chem. 144 (1999) 220–223.
[10] M. Toupin, T. Brousse, D. Bélanger, Chem. Mater. 14 (2002) 3946–3952.
[11] H. Kim, B.N. Popov, J. Electrochem. Soc. 150 (2003) D56–D62.
[12] M. Toupin, T. Brousse, D. Bélanger, Chem. Mater. 16 (2004) 3184–3190.
[13] S.C. Pang, M.A. Anderson, T.W. Chapman, J. Electrochem. Soc. 147 (2000) 444–450.
[14] S.C. Pang, M.A. Anderson, J. Mater. Res. 15 (2000) 2096–2106.
[15] Y.U. Jeong, A. Manthiram, J. Electrochem. Soc. 149 (2002) A1419–A1422.
[16] R.N. Reddy, R.G. Reddy, J. Power Sources 124 (2003) 330–337.
[17] J.N. Broughton, M.J. Brett, Electrochem. Solid-State Lett. 5 (2002) A279–A282.
[18] B. Djurfors, J.N. Broughton, M.J. Brett, D.G. Ivey, J. Mater. Sci. 38 (2003) 4817–4830.
[19] V. Subramanian, H. Zhu, R. Vajtai, P.M. Ajayan, B. Wei, J. Phys. Chem. B 109 (2005) 20207–20214.
[20] C.C. Hu, Y.T. Wu, K.H. Chang, Chem. Mater. 20 (2008) 2890–2894.
[21] J.K. Chang, Y.L. Chen, W.T. Tsai, J. Power Sources 135 (2004) 344–353.
[22] J.K. Chang, W.T. Tsai, J. Electrochem. Soc. 152 (2005) A2063–A2068.
[23] S. Devaraj, N. Munichandraiah, J. Electrochem. Soc. 154 (2007) A80–A88.
[24] C.K. Lin, K.H. Chuang, C.Y. Lin, C.Y. Tsay, C.Y. Chen, Surf. Coat. Technol. 202 (2007) 1272–1276.
[25] K.R. Prasad, N. Miura, Electrochem. Commun. 6 (2004) 1004–1008.
[26] P.Y. Chuang, C.C. Hu, Mater. Chem. Phys. 92 (2005) 138–145.
[27] J.K. Chang, M.T. Lee, C.H. Huang, W.T. Tsai, Mater. Chem. Phys. 108 (2008) 124–131.
[28] J.K. Chang, W.C. Hsieh, W.T. Tsai, J. Alloys Comp. 461 (2008) 667–674.
[29] M. Nakayama, A. Tanaka, Y. Sato, T. Tonosaki, K. Ogura, Langmuir 21 (2005) 5907–5913.
[30] M. Nakayama, A. Tanaka, S. Konishi, K. Ogura, J. Mater. Res. 19 (2004) 1509–1515.
[31] M.T. Lee, J.K. Chang, W.T. Tsai, J. Electrochem. Soc. 154 (2007) A875–A881.
[32] C. Tsang, J. Kim, A. Manthiram, J. Solid State Chem. 137 (1998) 28–32.
[33] H. Ikeda, US Patent 4,133,856.
[34] M. Chigane, M. Ishikawa, J. Electrochem. Soc. 147 (2000) 2246–2251.
[35] M. Chigane, M. Ishikawa, M. Izaki, J. Electrochem. Soc. 148 (2001) D96–D101.
[36] J.C. Carver, G.K. Schweitzer, T.A. Carlson, J. Chem. Phys. 57 (1972) 973–982.
[37] M. Oku, K. Hirokawa, S. Ikeda, J. Electron Spectrosc. Relat. Phenom. 7 (1975) 465–473.
[38] N.S. McIntyre, D.G. Zetaruk, Anal. Chem. 49 (1977) 1521–1529.
[39] T.C. Lin, G. Seshadri, J.A. Kelber, Appl. Surf. Sci. 119 (1997) 83–92.
[40] S.B. Kanungo, K.M. Parida, B.R. Sant, Electrochim. Acta 26 (1981) 1147–1156.
[41] D.A. Mckeown, P.L. Hagans, L.P.L. Carette, A.E. Russell, K.E. Swider, D.R. Rolison, J. Phys. Chem. B 103 (1999) 4825–4832.
[42] J.K. Chang, M.T. Lee, W.T. Tsai, J. Power Sources 166 (2007) 590–594.
[43] K.W. Nam, M.G. Kim, K.B. Kim, J. Phys. Chem. C 111 (2007) 749–758.